Available online at www.sciencedirect.com
SCIENCE DIRECT
ELSEVIER
European Journal of Mechanics B/Fluids 24 (2005) 237–254
EUROPEAN JOURNAL OF MECHANICS B/FLUIDS

Revisiting the stability of pulsatile pipe flow

F. Fedele [a,*], D.L. Hitt [b], R.D. Prabhu [b]

[a] *Department of Civil and Environmental Engineering, University Vermont, Burlington, VT 05405, USA*
[b] *Department of Mechanical Engineering, University of Vermont, Burlington, VT 05405, USA*

Received 17 November 2003; received in revised form 3 July 2004; accepted 19 July 2004

Available online 18 September 2004

Abstract

We revisit the problem of the stability of pulsatile pipe flow for axisymmetric perturbations. In contrast to the earlier approach based on the Chebyshev expansion for the spatial discretization [J. Appl. Mech. ASME 53 (1986) 187], we use the set of the eigenfunctions derived from the longwave limit of the Orr–Sommerfeld equation. We show that the Orr–Sommerfeld basis gives greater accuracy than the Chebyshev basis if fewer terms are used in the Galerkin expansion. For the time evolution of the flow perturbation, instead of the usual Floquet analysis, a different representation for the solution of the periodic system of linear differential equations is employed. We found that the flow structures corresponding to the largest energy growth are toroidal vortex tubes. They are stretched by the shear stress of the mean flow so that a maximum energy growth occurs. The flow perturbation subsequently decays due to viscous effects. The maximum energy growth is then evaluated over a range of Reynolds and Womersley numbers. Asymptotic solutions provided for the longwave limit as well as the limit of large Womersley numbers agree well with the numerical results, confirming the known linear stability of the flow.

Keywords: Stability; Pulsatile pipe flow; Orr–Sommerfeld operator; Galerkin projection; Non-normality; Vortex tubes; Energy growth

1. Introduction

The study of pulsatile tube flow appears to have been first considered in the context of arterial hemodynamics in the mid-1950s. Womersley and co-workers obtained an exact solution of the Navier–Stokes equations for the fully-developed velocity profile of a oscillatory, incompressible flow in a circular tube [1,2]. The stability and behavior of arterial blood flow in response to perturbations (receptivity) – whether arising from a cardiac fluctuation or a vessel wall non-uniformity or constriction – can have significant implications for altered vascular wall shear stresses and overall vascular impedance. For example, changes in normal wall shear stress distributions are believed to play a role in atherogenesis whereas a transition to turbulent flow within a large vessel can lead to substantial increases in flow resistance and increased cardiac load [3].

Pulsatile flow has also recently found renewed significance in its application to MEMS microfluidic engineering applications. A common feature of many of the microfluidic devices described in the literature that incorporate micro-scale pumping is that the flow is a pulsatile one [4,5]. The case of flow pulsations as a potential laminar mixing strategy for MEMS devices have also been examined in [6,7]. The relevance of pulsatile flow for arterial flows and certain microfluidic applications has thus provided the motivation of the present study in which we re-examine its stability characteristics.

* Corresponding author. Tel: +1-802-656-8140; fax: +1-802-656-1102.
E-mail address: ffedele@emba.uvm.edu (F. Fedele).

0997-7546/$ – see front matter
doi:10.1016/j.euromechflu.2004.07.005

The linear stability of the limiting case of steady Poiseuille flow in a pipe has been investigated extensively by a number of authors [8–15]. Such an analysis shows that all the eigenmodes are damped, although an initial energy growth of the flow perturbation can occur due to the non-normality of the Orr–Sommerfeld operator (i.e. the operator does not commute with its adjoint). For a non-normal operator [16,17] the associated eigenmodes do not exhibit orthogonality and consequently their superposition can result in an energy growth.

In this paper we revisit the problem of the linear stability of pulsatile pipe flow. We shall consider only axisymmetric perturbations and study their transient energy growth, although we point out that non-axisymmetric disturbances may likely exist having higher energy growth as for the case of steady pipe flow [10,17]. The starting point is the fourth-order Orr–Sommerfeld equation which is satisfied by the Stokes stream function for axisymmetric flow perturbations [18]. We shall consider the approach proposed in [14,15] where the set of eigenfunctions of a simplified Orr–Sommerfeld operator is used for the solution of the Orr–Sommerfeld equation by the Galerkin method. In contrast to the earlier approach [19] in which a Chebyshev expansion was used, our spatial discretization is based on the eigenfunctions derived from the long-wave limit of the Orr–Sommerfeld equation. We note that these eigenfunctions are essentially the eigenmodes of the Stokes flow for a pipe. The comparison of the two eigenbasis shows that for smaller number of terms $N \sim 15$–20 in the Galerkin expansion, the Orr–Sommerfeld eigenbasis gives smaller relative error then the Chebyshev basis, although it is well known that the Chebyshev basis gives smaller error than any power of N^{-1} asymptotically for $N \to \infty$. Nevertheless, the use of the Orr–Sommerfeld basis seems to be a very good candidate for the construction of lower order models by the Galerkin method: fewer eigenmodes would be sufficient to retain relatively greater accuracy than the Chebyshev basis.

For the time evolution of the flow perturbation, instead of the usual Floquet analysis, a different representation for the solution of the periodic system of linear differential equations is employed. The interested reader may refer to Refs. [20–25] for other time-dependent flow stability analyses. An excellent summary on the stability of time-periodic flows is found in [26].

For the case of axisymmetric perturbations, it has been found in this work that the flow structures giving the largest energy growth are toroidal vortex tubes. These axisymmetric flow structures are stretched by the shear stress of the mean flow along the streamwise direction and reach a point of maximum energy growth. Beyond this point a decay occurs due to viscous effects. Maximum energy growth of the flow perturbation has been evaluated over a range of Reynolds and Womersley numbers; the parametric regime considered has been chosen in part due to their relevance to arterial blood flow and also to microfluidic applications. Our numerical results are found to be in good agreement with asymptotic solutions obtained for the long-wave limit as well as the limit of large Womersley numbers.

The determination of the initial conditions which give rise to the maximum energy growth appears to be relevant, if transition to turbulence is thought as emanating from nonmodal energy growth mechanisms, i.e. 'bypass transition' (see [27, p. 402] and [28]). Another viewpoint on the transition to turbulence has been proposed in [29–31]; here, a specific feedback mechanism to transition in channel flows has been identified based on a self-sustaining process. This approach has led to the discovery of exact travelling wave solutions for pipe flows [32,33].

Recent experimental results of Hof et al. [34] suggest that both nonmodal energy growth and self-sustaining mechanism could be important to understand pipe flow transition. In their experimental work it has been found that the finite amplitude of the perturbation necessary to trigger transition in a pipe flow scales as $\mathrm{O}(\mathsf{Re}^{-1})$ with Re the Reynolds number. As reported by Hof et al. [34] regarding the exponent of this scaling, "*the exponent ... is in agreement with recent estimates for pipe flows where transient growth plays a role. The exponent also indicates a generic transition so that a challenge to theory is to provide a more definitive indicator which will permit a distinction between competing ideas to be made*".

Along these lines, we believe that the semi-analytical approach presented in this paper provides a framework for examining non-axisymmetric perturbations and their linear or nonlinear space-time dynamics. The highlight of the present work is the possibility of constructing Galerkin lower order models for pipe flows using fewer eigenmodes yet retaining greater accuracy.

2. The Orr–Sommerfeld equation for perturbed, oscillatory pipe flow

Consider the pulsatile flow dynamics in a pipe of circular cross section of radius R driven by an imposed periodic pressure gradient $\partial P/\partial z$. The fully-developed streamwise velocity $W(r,t)$ satisfies the following initial boundary value problem

$$\frac{\partial W}{\partial t} - \nu \frac{1}{r}\frac{\partial}{\partial r}\left(r\frac{\partial W}{\partial r}\right) = -\frac{1}{\rho}\frac{\partial P}{\partial z}, \qquad \frac{\partial P}{\partial z} = -\left[K_0 + K_\omega \exp(\mathrm{i}\omega t)\right] \tag{1}$$

with the no-slip condition at the boundary of the pipe, and the boundedness of the velocity field at the centerline of the tube. The solution for the radial velocity profile $W(r,t)$ is given by [1,2]

$$W(r,t) = \frac{K_0}{4\mu}(R^2 - r^2) + \frac{R^2}{\mu \mathsf{Wo}^2 \mathrm{i}}\left[1 - \frac{J_0(\frac{r}{R}\mathrm{i}^{3/2}\mathsf{Wo})}{J_0(\mathrm{i}^{3/2}\mathsf{Wo})}\right] K_\omega \exp(\mathrm{i}\omega t), \tag{2}$$

where R is the tube radius, J_0 is the Bessel function of the first kind of order zero [35], μ is the viscosity, and the parameter Wo, known as the Womersley number, is defined by $\mathrm{Wo} = \sqrt{\rho\omega R^2/\mu}$. It may be interpreted as either the ratio of oscillatory inertia to viscous forces or as a Reynolds number for the flow using ωR as the velocity scale. Still a third interpretation is as a measure of the ratio of the tube radius to the Stokes layer thickness $\delta_s = (\nu/\omega)^{1/2}$.

In order to study the stability of the basic flow field (2), the axisymmetric velocity perturbation ($u_r = u, u_\theta = 0, u_z = w$) is superimposed onto the basic flow,

$$u_r = u(z,r,t), \quad u_\theta = 0, \quad u_z = W(r,t) + w(z,r,t), \quad \tilde{p} = p(z,r,t) + P(z,t). \tag{3}$$

Here, (z, r, θ) define a cylindrical coordinate system with z-axis along the streamwise direction, (u_r, u_θ, u_z) are the radial, azimuthal and streamwise velocity components and $\tilde{p}$ is the pressure. The velocity field (3) has to satisfy the incompressible Navier–Stokes equations

$$\begin{cases} \dfrac{Du_r}{Dt} = \dfrac{u_\theta^2}{r} - \dfrac{1}{\rho}\dfrac{\partial\tilde{p}}{\partial r} + \nu\left(\nabla^2 u_r - \dfrac{u_r}{r^2} - \dfrac{2}{r^2}\dfrac{\partial u_\theta}{\partial\theta}\right), \\ \dfrac{Du_\theta}{Dt} = -\dfrac{1}{\rho r}\dfrac{\partial\tilde{p}}{\partial\theta} + \nu\left(\nabla^2 u_\theta + \dfrac{2}{r^2}\dfrac{\partial u_r}{\partial\theta} - \dfrac{u_\theta}{r^2}\right), \\ \dfrac{Du_z}{Dt} = -\dfrac{1}{\rho}\dfrac{\partial\tilde{p}}{\partial z} + \nu\nabla^2 u_z, \\ \dfrac{\partial u_r}{\partial r} + \dfrac{u_r}{r} + \dfrac{1}{r}\dfrac{\partial u_\theta}{\partial\theta} + \dfrac{\partial u_z}{\partial z} = 0, \end{cases} \tag{4}$$

where $D(\cdot)/Dt, \nabla^2(\cdot)$ are the material derivative and the Laplacian operator in cylindrical coordinates respectively. Substituting the velocities (3) into Eq. (4) and neglecting nonlinear terms, yield the following equations

$$\begin{cases} \dfrac{\partial u}{\partial t} + W\dfrac{\partial u}{\partial z} = -\dfrac{1}{\rho}\dfrac{\partial p}{\partial r} + \nu\left(\dfrac{1}{r}\dfrac{\partial}{\partial r}\left(r\dfrac{\partial u}{\partial r}\right) + \dfrac{\partial^2 u}{\partial z^2} - \dfrac{u}{r^2}\right), \\ \dfrac{\partial w}{\partial t} + u\dfrac{\partial W}{\partial r} + W\dfrac{\partial w}{\partial z} = -\dfrac{1}{\rho}\dfrac{\partial p}{\partial z} + \nu\left(\dfrac{1}{r}\dfrac{\partial}{\partial r}\left(r\dfrac{\partial w}{\partial r}\right) + \dfrac{\partial^2 w}{\partial z^2}\right), \\ \dfrac{1}{r}\dfrac{\partial}{\partial r}(ru) + \dfrac{\partial w}{\partial z} = 0 \end{cases} \tag{5}$$

governing the linear dynamics of the axisymmetric flow perturbation (u, w, p). We assume periodicity along the streamwise direction and let α denote the streamwise wave number. The Stokes stream function $\Psi(r,z,t) = \psi(r,t)\mathrm{e}^{\mathrm{i}\alpha z}$ allows the following representation of the radial and streamwise velocity components of the perturbation

$$u = -\frac{1}{r}\frac{\partial\Psi}{\partial z} = -\frac{\psi(r,t)}{r}\mathrm{i}\alpha\mathrm{e}^{\mathrm{i}\alpha z}, \qquad w = \frac{1}{r}\frac{\partial\Psi}{\partial r} = \frac{1}{r}\frac{\partial\psi}{\partial r}\,\mathrm{e}^{\mathrm{i}\alpha z} \tag{6}$$

and the condition of incompressibility is automatically satisfied in Eq. (5). Eliminating the perturbation pressure p from the two first equations of (5) and using Eq. (6), the following Orr–Sommerfeld equation for ψ can be obtained (see also [8–18])

$$\begin{cases} \mathcal{L}\psi_t - W\mathrm{i}\alpha^3\psi + \mathrm{i}\alpha(-\psi\mathcal{L}W + W\mathcal{L}\psi) = \mathrm{Re}^{-1}\mathcal{L}^2\psi, \\ \dfrac{\psi(r,t)}{r} < \infty, \quad \dfrac{1}{r}\dfrac{\partial\psi}{\partial r} < \infty \quad \text{as } r \to 0^+, \\ \psi(1,t) = \dfrac{\partial\psi}{\partial r}(1,t) = 0. \end{cases} \tag{7}$$

Here, the differential operator is defined by

$$\mathcal{L} = \frac{\partial^2}{\partial r^2} - \frac{1}{r}\frac{\partial}{\partial r} - \alpha^2$$

and the boundary conditions reflect the boundedness of the flow at the centerline of the pipe and the no-slip condition at the wall. In order to derive Eq. (7) the time, radial lengths, streamwise lengths and velocities have been scaled with T, R, L, U_0 respectively. Here, $T = R/U_0$ is a convective time scale, R is the tube radius, $L = 2\pi/\alpha$ is the wavelength of the perturbation and U_0 a characteristic velocity. The Reynolds and Strouhal numbers are defined as

$$\mathrm{Re} = \frac{U_0 R}{\nu}, \qquad \mathrm{St} = \omega T. \tag{8}$$

The basic velocity field W (see Eq. (2)) is in the dimensionless form

$$W(r,t) = W_0 + W_1 \exp(\mathrm{i}t\,\mathsf{St}) \tag{9}$$

and the functions W_0 and W_1 are given by

$$W_0 = \Lambda_0(1-r^2), \qquad W_1 = \Lambda_1 \frac{1}{\mathrm{i}}\left[1 - \frac{J_0(\mathrm{i}^{3/2}\,\mathsf{Wo}\,r)}{J_0(\mathrm{i}^{3/2}\,\mathsf{Wo})}\right], \tag{10}$$

where the non-dimensional amplitudes Λ_0 and Λ_1 have expression as

$$\Lambda_0 = \frac{K_0 R^2}{4\mu U_0}, \qquad \Lambda_1 = \frac{K_\omega R^2}{\mu\,\mathsf{St}\,\mathsf{Re}\,U_0}.$$

In the following it is chosen $U_0 = K_0 R^2/4\mu$ (characteristic velocity of steady Poiseuille flow) which yields $\Lambda_0 = 1$ and $\Lambda_1 = 4K_\omega/(K_0\,\mathsf{St}\,\mathsf{Re})$.

The flows considered in this paper are characterized by the numbers $\mathsf{Re} = 50$–5000 and $\mathsf{Wo} = 10$–30; the corresponding frequency regime is given by Strouhal numbers $\mathsf{St} \simeq 0.1$–20. This parametric regime was chosen so as to include cases of arterial blood flows as well as MEMS-based pumping.

3. Galerkin method

We now derive the time-periodic system of first order linear differential equations which governs the dynamics of the flow perturbation. Following the approach used in [14,15] where the eigenmodes of a simplified Orr–Sommerfeld operator are considered, for the spatial discretization of the Orr–Sommerfeld equation (7) we use a finite set of the eigenfunctions of the long-wave limit Orr–Sommerfeld operator (i.e. Orr–Sommerfeld basis). Other eigenbasis can be chosen for the spatial Galerkin projection, as for the example Chebyshev polynomials. In Appendix D we report numerical results showing that the Orr–Sommerfeld basis gives better accuracy than the Chebyshev basis if few terms $N \sim 15$–20 in the Galerkin expansion are used.

3.1. The long-wave Orr–Sommerfeld basis

Exact solutions of the Orr–Sommerfeld equation are difficult to obtain for an arbitrary wave number α. In the limit of $\alpha \to 0$, which represents the case of a long-wave perturbation, Eq. (7) admits the simple expansion

$$\tilde{\psi}(r,t) = \sum_{n=1}^{\infty} a_n \phi_n(r) \exp(-\lambda_n t).$$

The set of coefficients $\{a_n\}_{n=1}^{\infty}$ is defined by the initial conditions and the set of eigenfunctions $\{\phi_n(r)\}_{n=1}^{\infty}$[1] and eigenvalues $\{\lambda_n\}_{n=1}^{\infty}$ satisfy the eigenvalue problem

$$\begin{cases} \tilde{\mathcal{L}}^2\phi_n = -\mathsf{Re}\,\lambda_n \tilde{\mathcal{L}}\phi_n, \\ \dfrac{1}{r}\phi_n < \infty, \quad \dfrac{1}{r}\dfrac{\partial\phi_n}{\partial r} < \infty, \quad r \to 0^+, \\ \phi_n = \dfrac{\partial\phi_n}{\partial r} = 0 \quad \text{at } r = 1. \end{cases} \tag{11}$$

Here, $\tilde{\mathcal{L}} = r\partial/\partial r(r^{-1}\partial/\partial r)$ is a reduced operator and the eigenvalues are given by $\lambda_n = \chi_n^2/\mathsf{Re}$ where χ_n are the roots of $J_2(\chi) = 0$. One readily finds (see Appendix A for details)

$$\phi_n(r) = \frac{\sqrt{2}}{\chi_n} r\left(r - \frac{J_1(\chi_n r)}{J_1(\chi_n)}\right), \tag{12}$$

where $J_1(r)$and $J_2(r)$are the Bessel functions of first kind of order 1 and 2, respectively [35]. The first six eigenfunctions, shown in Fig. 1, exhibit the characteristic behavior of Bessel's functions: increasing number of extrema and monotonically decreasing maxima. Since the perturbation is bounded for $r \to 0^+$, this implies $\phi_n = \partial\phi_n/\partial r = 0$ at $r = 0$, and this may be verified directly from Eq. (12).

[1] Note that this set represents the eigenmodes of the Stokes flow for a pipe.

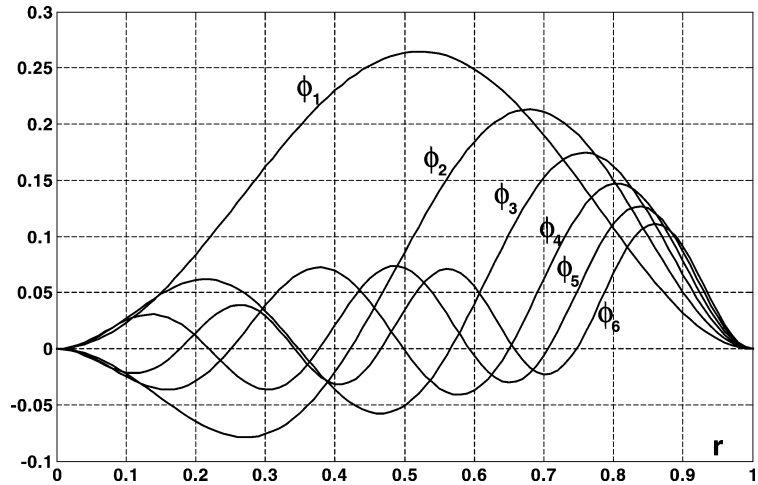

Fig. 1. The first 6 long-wave Orr–Sommerfeld eigenfunctions.

The function space $\mathcal{F} = \text{span}(\phi_1, \ldots, \phi_n, \ldots)$ with the following inner product

$$\langle f, g\rangle = -\int_0^1 f\,\tilde{\mathcal{L}} g \frac{\mathrm{d}r}{r} = \int_0^1 \frac{\partial f}{\partial r}\frac{\partial g}{\partial r}\frac{\mathrm{d}r}{r}, \tag{13}$$

is a Hilbert space and the set of eigenfunctions $\{\phi_n\}_{n=1}^{\infty}$ is a complete orthonormal set. We shall refer to the set $\{\phi_n\}_{n=1}^{\infty}$ as the Orr–Sommerfeld basis. The inner product (13) induces the following norm

$$\|f\|^2 = \langle f, f^*\rangle = \int_0^1 \frac{\partial f}{\partial r}\frac{\partial f^*}{\partial r}\frac{\mathrm{d}r}{r} = 2\mathcal{E}(f,t)|_{\alpha=0}.$$

This norm is twice the long-wave limit of the energy $\mathcal{E}(f,t)$ of the axisymmetric velocity field $u_f = -\frac{f}{r}\mathrm{i}\alpha \mathrm{e}^{\mathrm{i}\alpha z}$ and $w_f = \frac{1}{r}\frac{\partial f}{\partial r}\mathrm{e}^{\mathrm{i}\alpha z}$ (see Eq. (6)), defined as

$$\mathcal{E}(f,t) = \frac{1}{2}\int_0^1 (u_f u_f^* + w_f w_f^*)\,\mathrm{d}r = \frac{1}{2}\int_0^1 \left(\frac{\partial f}{\partial r}\frac{\partial f^*}{\partial r} + \alpha^2 f\ f^*\right)\frac{\mathrm{d}r}{r}. \tag{14}$$

3.2. Galerkin projection

Consider now a complete basis $\{h_k(r)\}_{k=1}^{\infty}$ for the function space $\mathcal{F}$ where $\{h_k(r)\}_{k=1}^{\infty}$ can be the Orr–Sommerfeld basis $\{\phi_n\}_{n=1}^{\infty}$ or any other basis. Let us define its finite dimensional subspace $\widehat{\mathcal{F}} = \text{span}[h_1(r), h_2(r), \ldots, h_N(r)]$, where N is the number of function basis. In order to solve the Orr–Sommerfeld equation (7) we seek an approximation stream function $\hat{\psi}(r,t) \in \widehat{\mathcal{F}}$ as

$$\hat{\psi}(r,t) = \sum_{k=1}^{N} a_k(t) h_k(r), \tag{15}$$

where $\{a_k(t)\}_{n=1}^{N}$ are time-dependent coefficients to be determined. Under this expansion the boundary conditions in Eq. (7) are automatically satisfied. To derive the equations for $\{a_k(t)\}_{n=1}^{N}$ we shall project the Orr–Sommerfeld equation (7) onto the approximation function space $\widehat{\mathcal{F}}$. Using the inner product in Eq. (13), the n-th projection of the Orr–Sommerfeld equation in Eq. (7) appears as

$$-\int_0^1 \left[\mathcal{L}\hat{\psi}_t - W\mathrm{i}\alpha^3\hat{\psi} + \mathrm{i}\alpha(-\hat{\psi}\mathcal{L}W + W\mathcal{L}\hat{\psi}) - \frac{1}{\mathrm{Re}}\mathcal{L}^2\hat{\psi}\right] h_n \frac{\mathrm{d}r}{r} = 0. \tag{16}$$

By substituting the expansion (15) into Eq. (16), it is possible to show that the set of time-varying functions $\{a_n(t)\}_{n=1}^{N}$ satisfies a finite system of periodic, first-order linear ordinary differential equations. In matrix notation, the system is given by

$$\mathbf{M}\frac{\mathrm{d}\mathbf{a}}{\mathrm{d}t} = \left[\mathbf{K} + \mathbf{H}\exp(\mathrm{i}t\,\mathsf{St})\right]\mathbf{a}. \tag{17}$$

Here, $\mathbf{a}(t)$ is a column vector of dimension N whose n-th component is $a_n(t)$ and the constant matrices $\mathbf{M}$, $\mathbf{K}$, $\mathbf{H}$ of dimension $(N \times N)$ are defined in Appendix B. From Eq. (14) the energy of the velocity field associated to the approximation stream function $\hat{\psi}$ is expressed as

$$\mathcal{E}(\psi, t) = \frac{1}{2}\mathbf{a}^*(t)\mathbf{M}\mathbf{a}(t), \tag{18}$$

where $\mathbf{a}^*$ denotes the Hermitian conjugate. Since the energy is a positive definite scalar quantity, this implies that the matrix $\mathbf{M}$ has to be positive definite and therefore its inverse exists. Thus Eq. (17) can be rewritten as

$$\frac{\mathrm{d}\mathbf{a}}{\mathrm{d}t} = \left[\mathbf{M}^{-1}\mathbf{K} + \mathbf{M}^{-1}\mathbf{H}\exp(\mathrm{i}t\,\mathsf{St})\right]\mathbf{a}. \tag{19}$$

The fundamental matrix $\mathbf{G}(t)$ satisfies the system (19) with initial conditions $\mathbf{G}(0) = \mathbf{I}$, where $\mathbf{I}$ is the $N \times N$ identity matrix.

4. The energy growth

The time evolution of $\mathbf{a}(t)$, for any t, depends entirely on the fundamental matrix $\mathbf{G}(\tau)$ for the system (19), evaluated only on the interval $\tau \in [0, \mathsf{T}]$ where $\mathsf{T} = 2\pi/\mathsf{St}$ is the dimensionless period of oscillations. By decomposing the time as $t = \tau + m\mathsf{T}$ with m an integer, the solution can be written as

$$\mathbf{a}(t) = \mathbf{G}(\tau)\mathbf{G}^m(\mathsf{T})\mathbf{a}(0), \quad \tau \in [0, \mathsf{T}], \tag{20}$$

where the vector $\mathbf{a}(0)$ defines the initial conditions. Extensive computations (e.g. Runge–Kutta method) show that the matrix $\mathbf{G}(\mathsf{T})$ has distinct eigenvalues $\{\mu_k\}_{k=1}^{N}$ (a.k.a. the characteristic multipliers) which allows the diagonalization

$$\mathbf{G}(\mathsf{T}) = \mathbf{Q}\exp(\boldsymbol{\Gamma}\mathsf{T})\,\boldsymbol{Q}^{-1}. \tag{21}$$

Although the columns of $\mathbf{Q}$ are linearly independent, they are in general not orthogonal; this is a consequence of the non-normality of the Orr–Sommerfeld operator. The diagonal entries of the matrix $\boldsymbol{\Gamma}$ are the characteristic exponents $\{\gamma_k\}_{k=1}^{N}$ which are related to the characteristic multipliers by

$$\gamma_k = \frac{\ln \mu_k}{\mathsf{T}}. \tag{22}$$

The solution is strictly stable if all the characteristic exponents γ_k lie strictly in the left hand part of the complex plane, i.e. $\mathrm{Re}(\gamma_k) < 0$.

The initial perturbation, defined by the vector $\mathbf{a}(0)$, is characterized by the stream function $\hat{\psi}(r, 0) = \sum_{k=1}^{N} a_k(0)h_k(r)$ (see Eq. (15)). Its energy growth $\mathcal{G}(t)$, at time t, can be evaluated by means of Eq. (18) as follows

$$\mathcal{G}(\mathbf{c}, t) = \frac{\mathcal{E}(\hat{\psi}, t)}{\mathcal{E}(\hat{\psi}, 0)} = \frac{\mathbf{a}(0)^*\mathbf{E}(t)\mathbf{a}(0)}{\mathbf{a}(0)^*\mathbf{E}(0)\mathbf{a}(0)}.$$

Here, the matrix $\mathbf{E}(t)$ is given by

$$\mathbf{E}(t) = \left[\mathbf{G}^m(\mathsf{T})\right]^*\mathbf{G}(\tau)^*\mathbf{M}\,\mathbf{G}(\tau)\,\mathbf{G}^m(\mathsf{T}). \tag{23}$$

The optimal initial condition $\mathbf{a}_{\mathrm{opt}}$ which gives the maximum growth $\mathcal{G}_{\mathrm{opt}}(t)$ attained at time t satisfies the following eigenvalue problem

$$\mathbf{E}(t)\mathbf{a}_{\mathrm{opt}} = \mathcal{G}_{\mathrm{opt}}(t)E(0)\mathbf{a}_{\mathrm{opt}}. \tag{24}$$

Note that $\mathcal{G}_{\mathrm{opt}}(t)$ as function of t, should be thought as the envelope of the energy evolution of individual optimal initial conditions $\mathbf{a}_{\mathrm{opt}}$ giving the maximum growth $\mathcal{G}_{\mathrm{opt}}(t)$ at time t (see also [36]). The largest energy growth $\mathcal{G}_{\max}$ for the pulsatile flow, attained at time $t = t_{\max}$, is then given by

$$\mathcal{G}_{\max} = \sup_{t\in[0,\infty)} \mathcal{G}_{\mathrm{opt}}(t). \tag{25}$$

Note that $\mathcal{G}_{\max}$ can be alternatively evaluated via an adjoint method as in [27,37,38].

For the case of steady Poiseuille flow the fundamental matrix is readily derived from Eq. (19) as

$$\mathbf{G}_{\mathrm{st}}(t) = \exp(t\mathbf{M}^{-1}\mathbf{K}). \tag{26}$$

The optimal energy growth $\mathcal{G}_{\mathrm{opt,\,st}}(t)$ at time t is then given by the following expression

$$\mathcal{G}_{\mathrm{opt,\,st}}(t) = \left\| \mathbf{G}^{*}_{\mathrm{st}}(t)\mathbf{M}\mathbf{G}_{\mathrm{st}}(t) \right\|, \tag{27}$$

where the matrix norm $\|\cdot\|$ can be evaluated by means of the singular value decomposition [27,36].

5. Results

As an example, consider an axial perturbation with wavenumber $\alpha = 1$ and a strongly pulsatile forcing of the basic flow characterized by the ratio $K_\omega/K_0 = 2$. We shall use the long-wave Orr–Sommerfeld basis with a Galerkin expansion consisting of $N = 30$ terms. We examine the stability of a basic pulsatile flow state characterized by $\mathsf{St} = 1$, and $\mathsf{Wo} = \sqrt{\mathsf{Re}}$. The characteristic exponents $\{\gamma_k\}_{k=1}^{N}$ (see Eq. (22)) are plotted in Fig. 2 in the complex plane for $\mathsf{Re} = 1500$. For comparison purposes, the plot of the eigenvalues of the steady Poiseuille flow is also shown in the figure. The real part of the characteristic exponents are slightly more negative than their steady counterparts, indicating that the pulsatile flow is slightly more stable than the steady Poiseuille flow [19]. The characteristic exponents having the highest damping in Fig. 2 are spurious due to the numerical error in evaluating the fundamental matrix $\mathbf{G}(\mathsf{T})$ by the Runge–Kutta method. These spurious modes are ignored in the evaluation of the energy growth.

A plot of $\mathcal{G}_{\mathrm{opt}}(t)$ vs. t is shown in Fig. 3 for $\mathsf{Re} = 3500$ and two different values of the Womersley number $\mathsf{Wo} = 10$ and 30. Due to the non-normality of the Orr–Sommerfeld operator, $\mathcal{G}_{\mathrm{opt}}(t)$ is not a monotonic decreasing function of the time t. It first increases towards a maximum $\mathcal{G}_{\max}$ and then decays. The details of the flow structures at the point of maximum energy growth $\mathcal{G}_{\max}$ attained at time $t = t_{\max}$ are shown in Figs. 4 and 5 for the corresponding Womersley number of 10 and 30 respectively. These structures are toroidal vortex tubes. They are relatively more stretched along the streamwise direction by the mean flow as the Womersley number Wo increases. The increased stretching of the flow structure implies an increased velocity field and a corresponding increased flow energy. This confirms the higher value of the maximum energy growth $\mathcal{G}_{\max}$ for the case of Womersley number $\mathsf{Wo} = 30$ as one can see from Fig. 3.

As an example of the time evolution of the flow perturbation, consider the initial condition giving the largest energy growth $\mathcal{G}_{\max}$ for the case of $\mathsf{Wo} = 20$ and $\mathsf{Re} = 1000$ (dimensionless period oscillation $\mathsf{T} = 18.2$). At time $t = 0$ the stream function of the initial flow perturbation is given in Fig. 6. As time evolves, the mean shear stress tends to stretch the vortex tubes, so that at time $t = t_{\max} = 11.8$ (see Fig. 7) the flow configuration is such that its energy growth attains a maximum ($\mathcal{G}_{\max} \simeq 1.5$). Beyond this time the vortex tubes tend to migrate closer to the centerline ($r = 0$) where the effectiveness of the shear stress is diminished. The flow structure then decays in time due to viscous effects as shown in Figs. 8 and 9.

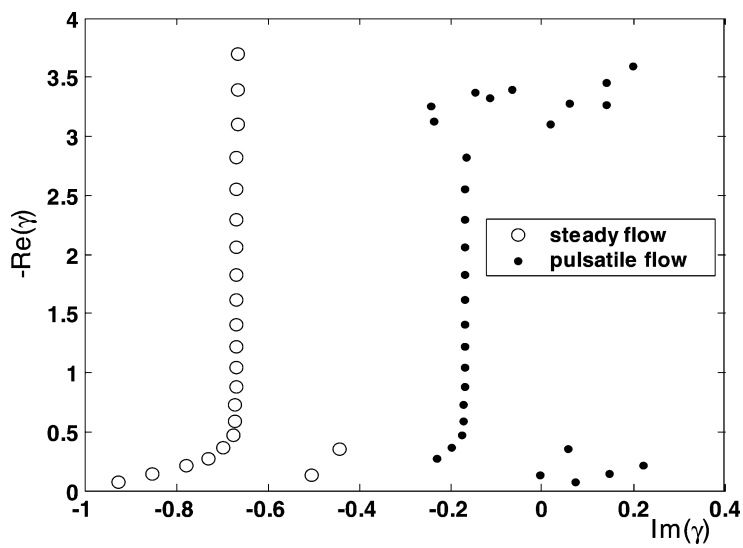

Fig. 2. Plots of the characteristic exponents $\{\gamma_k\}_{k=1}^{N}$ for $\mathsf{Re} = 1500$, $\mathsf{St} = 1$, $\mathsf{Wo} = \sqrt{\mathsf{Re}}$, $K_\omega/K_0 = 2$ and wavenumber $\alpha = 1$. For comparison purposes, the plot of the eigenvalues of the steady Poiseuille flow is also shown. (Galerkin expansion consisting of $N = 30$ terms.)

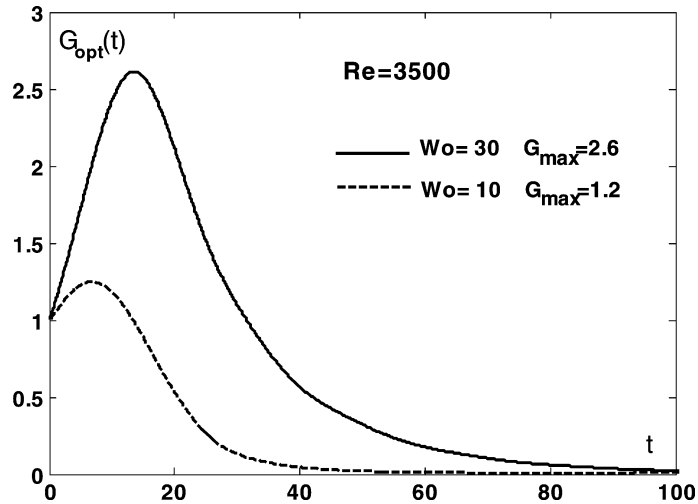

Fig. 3. The optimal energy growth $\mathcal{G}_{\mathrm{opt}}(t)$ as function of the time at which it occurs t ($\mathsf{Re} = 3500$ and $\mathsf{Wo} = 10, 30$). See Figs. 4, 5 for the corresponding stream function $\hat{\psi}(r, t)$ at time $t = t_{\max}$ when the max energy growth $\mathcal{G}_{\max}$ occurs.

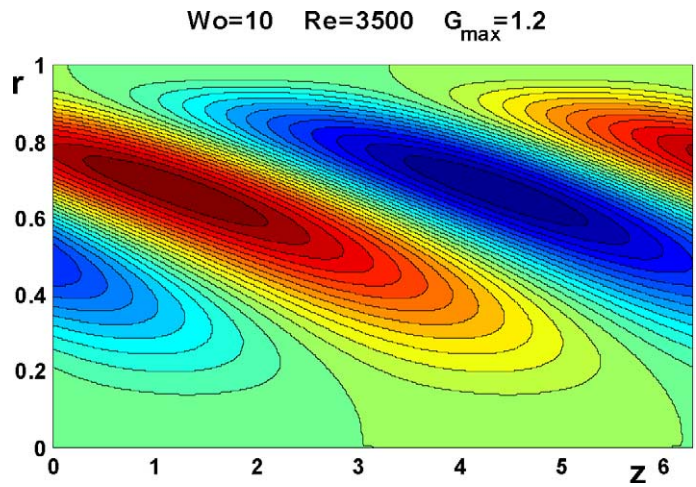

Fig. 4. Stream function of the optimal disturbance at time $t = t_{\max}$ when the max energy growth $\mathcal{G}_{\max} = 1.2$ occurs for $\mathsf{Wo} = 10$, $\mathsf{Re} = 3500$.

Finally the flow response to axisymmetric perturbations with wavenumber $\alpha = 1$ is summarized in Fig. 10. The maximum energy growth $\mathcal{G}_{\max}$ is plotted as a function of the Reynolds number Re in the range 50–5000, for values of the Womersley number Wo ranging between 10 to 30. The corresponding frequency regime is characterized by Strouhal numbers $\mathsf{St} \simeq 0.1$–20. For comparison, the plot of the maximum energy growth $\mathcal{G}_{\max,\,\mathrm{st}}$ for the case of steady Poiseuille flow is also displayed. For larger Wo, the stability characteristics of the steady Poiseuille flow are recovered. This is to be expected, since the amplitude of the pulsations scales as $\mathrm{O}(\mathsf{Wo}^{-2})$. For $\alpha = 1$ we find an upper bound of $\mathsf{Wo} \simeq 30$ beyond which the pulsatile forcing has negligible influence on the stability of the pulsatile flow. As the Womersley number is reduced, the flow perturbation is characterized by successively smaller maximum energy growth than its steady counterpart (see Fig. 10). This may provide a possible explanation for the observed suppression of the turbulence spots in pulsatile pipe flow transition for low frequency regimes (see [19] and references therein). The numerical results also provide a minimum Reynold number of $\mathsf{Re}_{\min} \simeq 370$ that has to be surpassed in order to yield an energy growth. This result is found to be independent of the Womersley number. It has been reported for steady Poiseuille flow that an energy growth occurs at the threshold Reynolds number $\alpha \mathsf{Re}_{\min} = 369.7$ (see [27], p. 117, Fig. 4.5). Thus, for $\alpha = 1$, we find that the minimum Reynolds number for steady and pulsatile cases are almost indistinguishable. This has immediate implications for pulsation-induced mixing on the micro-scale: for the typically low Reynolds numbers found in microchannel flows, it appears that linear perturbations to multi-fluid configurations will be ineffectual.

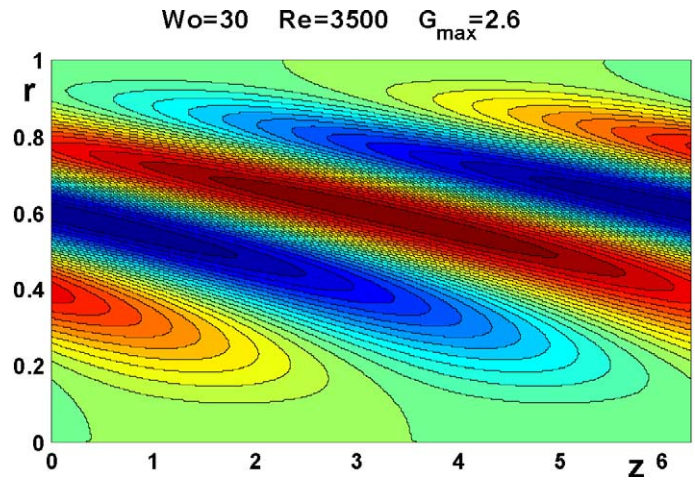

Fig. 5. Stream function of the optimal disturbance at time $t = t_{\max}$ when the max energy growth $\mathcal{G}_{\max} = 2.6$ occurs for $\mathrm{Wo} = 30$ and $\mathrm{Re} = 3500$.

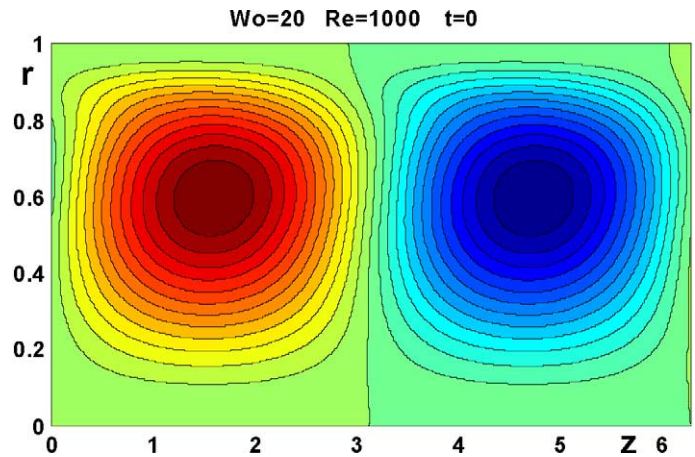

Fig. 6. Stream function of the optimal disturbance at time $t = 0$ for $\mathrm{Wo} = 20$ and $\mathrm{Re} = 1000$.

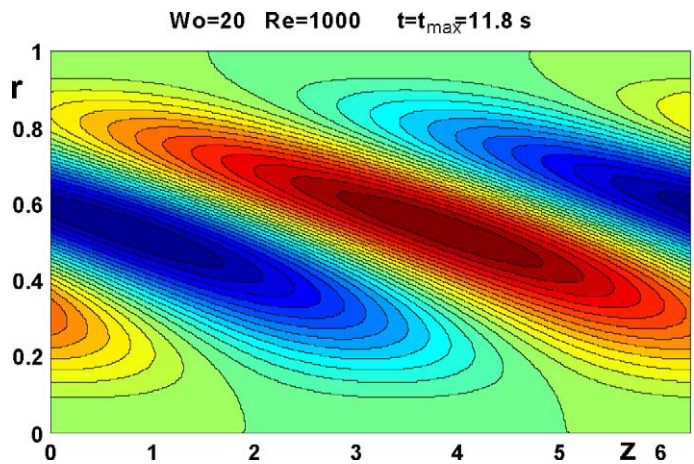

Fig. 7. Stream function of the optimal disturbance at time $t = t_{\max}$ for $\mathrm{Wo} = 20$ and $\mathrm{Re} = 1000$.

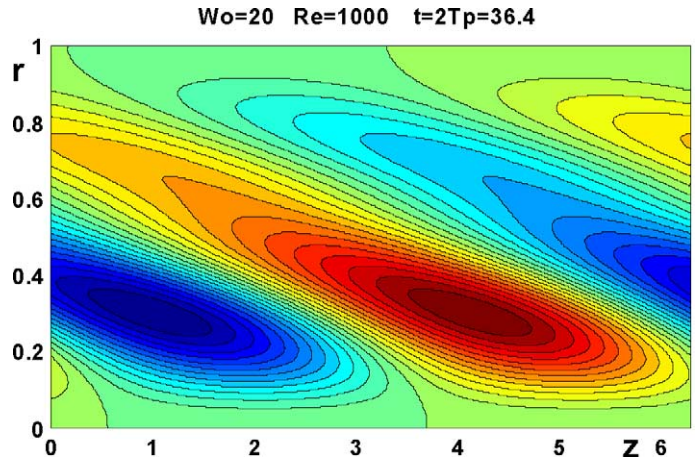

Fig. 8. Stream function of the optimal disturbance at time $t = 2\mathsf{T}$ for $\mathsf{Wo} = 20$ and $\mathsf{Re} = 1000$.

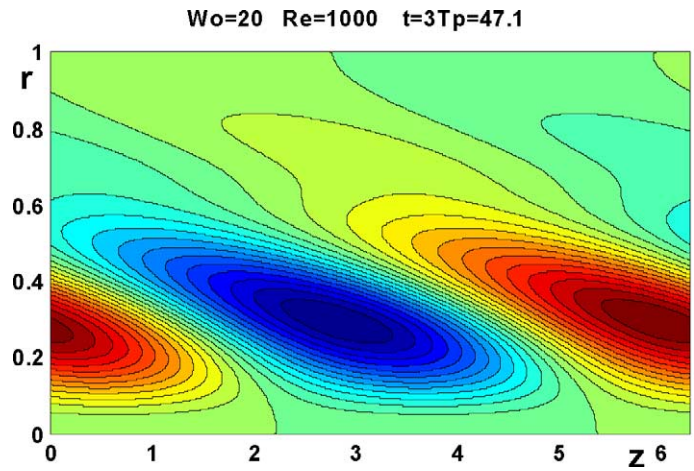

Fig. 9. Stream function of the optimal disturbance at time $t = 3\mathsf{T}$ for $\mathsf{Wo} = 20$ and $\mathsf{Re} = 1000$.

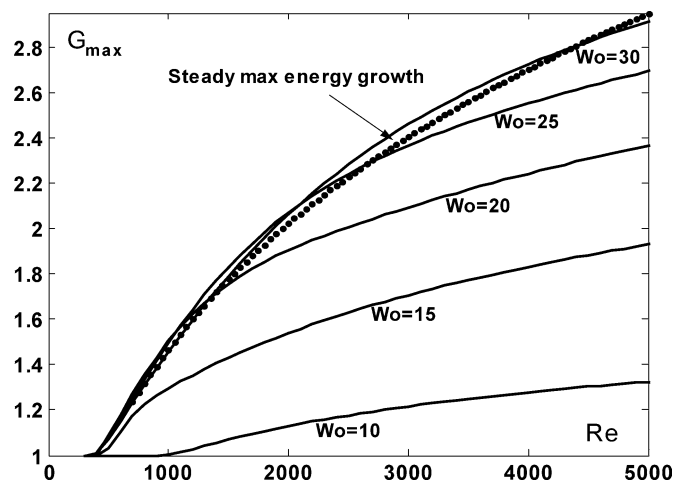

Fig. 10. Max energy growth $\mathcal{G}_{\max}$ as function of the Reynold number Re for different values of the Womersley number Wo. The plot of $\mathcal{G}_{\max,\,\mathrm{st}}$ for the case of steady Poiseille flow is also reported for comparison.

Table 1

$\tilde{\gamma}_k$ (asymptotic)	γ_k (numeric)	$\lvert 1-\tilde{\gamma}_k/\gamma_k\rvert$
$-0.0176-0.0818\mathrm{i}$	$-0.0198-0.0814\mathrm{i}$	0.0266
$-0.0473-0.0723\mathrm{i}$	$-0.0499-0.0738\mathrm{i}$	0.0341
$-0.0900-0.0696\mathrm{i}$	$-0.0907-0.0690\mathrm{i}$	0.0074
$-0.1460-0.0685\mathrm{i}$	$-0.1455-0.0682\mathrm{i}$	0.0031
$-0.2151-0.0679\mathrm{i}$	$-0.2145-0.0678\mathrm{i}$	0.0024
$-0.2973-0.0676\mathrm{i}$	$-0.2968-0.0675\mathrm{i}$	0.0016
$-0.3927-0.0673\mathrm{i}$	$-0.3923-0.0673\mathrm{i}$	0.0011
$-0.5013-0.0672\mathrm{i}$	$-0.5009-0.0672\mathrm{i}$	0.0007
$-0.6230-0.0671\mathrm{i}$	$-0.6227-0.0671\mathrm{i}$	0.0005
$-0.7579-0.0670\mathrm{i}$	$-0.7576-0.0670\mathrm{i}$	0.0004
$-0.9059-0.0670\mathrm{i}$	$-0.9057-0.0670\mathrm{i}$	0.0003
$-1.0671-0.0669\mathrm{i}$	$-1.0669-0.0669\mathrm{i}$	0.0002
$-1.2415-0.0669\mathrm{i}$	$-1.2413-0.0669\mathrm{i}$	0.0001
$-1.4290-0.0669\mathrm{i}$	$-1.4289-0.0669\mathrm{i}$	0.0001
$-1.6297-0.0668\mathrm{i}$	$-1.6296-0.0668\mathrm{i}$	0.0001

6. Asymptotic solutions

Analytical solutions of the system (19) can also be derived in two distinct and important limits. The first case is for a long-wave perturbation when $\alpha \ll 1$. The second solution is valid for high Womersley numbers ($\mathsf{Wo} \to \infty$).

6.1. The case of long-wave perturbations

In the long-wave limit there is a separation of the inertial, advection and viscous time scales, which suggests using a multiscale perturbation approach. Here, the streamwise wave number α serves as the small parameter in the multiscale expansion. Assume that Eq. (17) has been derived using the Orr–Sommerfeld basis. The long-wave limit solution (see Appendix C for details) for the fundamental matrix $\mathbf{G}(t)$ is given by

$$\mathbf{G}(t) = \exp\big[\big(\mathbf{K}_0 + \alpha\,\mathrm{diag}(\mathbf{K}_1) + \alpha^2\,\mathrm{diag}(\mathbf{K}_2 - \mathbf{M}_2\mathbf{K}_0)\big)t\big] \quad \text{as } \alpha/\mathsf{Wo}^2 \to 0. \tag{28}$$

We can conclude that in the limit of $\alpha/\mathsf{Wo}^2 \to 0$, the characteristic exponents $\{\gamma_k\}_{k=1}^N$ are equal to

$$\gamma_k = -\frac{\chi_k^2}{\mathsf{Re}}\left(1+\alpha^2\int_0^1 \phi_k^2\frac{\mathrm{d}r}{r}\right) - \frac{2}{\mathsf{Re}}\alpha^2 + \mathrm{i}\alpha\left(-1+\int_0^1 r\,\phi_k\tilde{\mathcal{L}}\phi_k\,\mathrm{d}r\right). \tag{29}$$

Note that Eq. (29) shows no dependence upon the oscillatory part of the flow (i.e. Wo) and gives the eigenvalues for the case of the steady Poiseuille flow. Thus in the long-wave limit, the perturbation is not affected by the pulsatile part of the flow if the wavelength of the disturbance L is much greater than the thickness δ_ω of the Stokes layer, i.e. $\alpha/\mathsf{Wo}^2 \to 0$.

Consider the pulsatile basic flow characterized by the numbers $\mathsf{Re} = 1500$, $\mathsf{St} = 1$, $\mathsf{Wo} = 38.7$ and $K_\omega/K_0 = 2$ and assume an axial perturbation with wavenumber $\alpha = 0.1$. We shall use the Galerkin expansion (15) consisting of $N = 30$ terms. In Table 1 it is shown a comparison between the eigenvalues obtained by numerically solving the fundamental matrix and the analytical eigenvalues (29). As one can see the agreement between numerical and analytical results is quite good.

6.2. The case of Womersley number $\mathsf{Wo} \to \infty$

The exact analytical solution of the system (19) can be obtained provided the two matrices $\mathbf{M}^{-1}\mathbf{K}$ and $\mathbf{M}^{-1}\mathbf{H}$ commute. In general, these two matrices do not commute, except for case of large Womersley numbers ($\mathsf{Wo} \to \infty$). In this limit, the amplitude W_1 of the oscillatory part of the basic flow (9) tends to be nearly uniform, since the thickness of the Stokes boundary layer tends to zero. The following asymptotic expression[2] for W_1 then holds

$$W_1 \simeq \widetilde{W}_1 = \frac{1}{\mathsf{Wo}^2}\frac{4K_\omega}{\mathrm{i}K_0} \quad \text{as } \mathsf{Wo} \to \infty. \tag{30}$$

[2] In Eq. (10), for fixed radius r, if $\mathsf{Wo} \to \infty$ the second term in the square brackets, involving Bessel's functions, goes to zero.

This implies that the matrix **H** (see Eq. (19) and Appendix D) simplifies as follows

$$\mathbf{H} \simeq -\mathrm{i}\alpha \widetilde{W}_1 \mathbf{M} \quad \text{as } \mathsf{Wo} \to \infty,$$

and the system (19) reduces to the form

$$\frac{\mathrm{d}\mathbf{a}}{\mathrm{d}t} = \left[\mathbf{M}^{-1}\mathbf{K} - \mathrm{i}\alpha \widetilde{W}_1 \mathbf{I} \exp(\mathrm{i}t\,\mathsf{St})\right]\mathbf{a}. \tag{31}$$

This system can be solved analytically since the scalar multiple of the identity matrix commutes with any other matrix. The solution is given by[3]

$$\mathbf{a}(t,\mathcal{T}) = \exp\left[\frac{4\alpha K_\omega t}{K_0 \mathsf{Wo}^2}\left(\frac{\sin\mathcal{T}}{\mathcal{T}} + \mathrm{i}\frac{\cos\mathcal{T}-1}{\mathcal{T}}\right)\right]\mathbf{G}_{\mathrm{st}}(t)\mathbf{a}(0) \quad \text{as } \mathsf{Wo} \to \infty, \tag{32}$$

where $\mathbf{G}_{\mathrm{st}}(t)$ is the fundamental matrix for the case of the steady Poiseuille flow (see Eq. (26)) and $\mathbf{a}(0)$ are appropriate initial conditions. Here the solution depends upon the time scale t and the long time scale $\mathcal{T} = t\,\mathsf{St}$. In Eq. (32), if also $\alpha/\mathsf{Wo}^2 \to 0$, then the exponential factor is almost equal to 1 and $\mathbf{G}_{\mathrm{st}}(t)$ tends to the long-wave limit solution (28).

The energy of the flow perturbation can be evaluated by means of Eq. (18) with the result

$$\mathcal{E}(t,\mathcal{T}) = \mathcal{E}_{\mathrm{st}}(t)\mathcal{E}_{\mathrm{osc}}(\mathcal{T}) \quad \text{as } \mathsf{Wo} \to \infty. \tag{33}$$

Here,

$$\mathcal{E}_{\mathrm{st}}(t) = \frac{1}{2}\mathbf{a}^*(0)\mathbf{G}^*_{\mathrm{st}}(t)\mathbf{M}\mathbf{G}_{\mathrm{st}}(t)\mathbf{a}(0)$$

is the energy of the flow perturbation in the steady Poiseuille flow and

$$\mathcal{E}_{\mathrm{osc}}(\mathcal{T}) = \exp\left(\frac{8\alpha K_\omega \mathsf{Re}}{K_0 \mathsf{Wo}^4}\sin\mathcal{T}\right).$$

Note that in this case the energy $\mathcal{E}(t,\mathcal{T})$ evolves on the time scale t as if the basic flow is steady. The effects due to the pulsatility of the basic flow are 'felt' on the long time scale $\mathcal{T}$ through the factor $\mathcal{E}_{\mathrm{osc}}(\mathcal{T})$. As t approaches infinity, $\mathcal{E}(t,\mathcal{T})$ goes to zero, confirming the stability of the pulsatile flow. However, an optimal energy growth

$$\mathcal{G}_{\mathrm{opt}}(t,\mathcal{T}) = \mathcal{G}_{\mathrm{opt,\,st}}(t)\mathcal{E}_{\mathrm{osc}}(\mathcal{T}) \quad \text{as } \mathsf{Wo} \to \infty, \tag{34}$$

can occur. Here, $\mathcal{G}_{\mathrm{opt,\,st}}(t)$ is the optimal energy growth for the steady Poiseuille flow at time t defined in Eq. (27). From Eq. (34), the following bound for the quotient η between the maximum energy growths $\mathcal{G}_{\max}$ and $\mathcal{G}_{\max,\,\mathrm{st}}$ is derived

$$\eta = \frac{\mathcal{G}_{\max}}{\mathcal{G}_{\max,\,\mathrm{st}}} \leqslant \exp\left(\frac{8\alpha K_\omega \mathsf{Re}}{K_0 \mathsf{Wo}^4}\right) \quad \text{as } \mathsf{Wo} \to \infty, \tag{35}$$

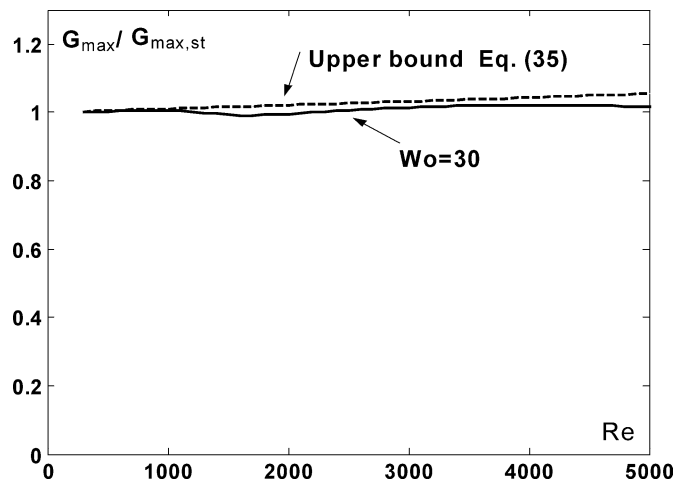

Fig. 11. Plots of the ratio η as a function of the Reynold number Re for $\mathsf{Wo} = 30$ and the upper bound defined in Eq. (35).

[3] The transformation $\mathbf{a}(t) = \exp[t\mathbf{M}^{-1}\mathbf{K}]\mathbf{b}(t)$ applied to Eq. (31) gives rise to a decoupled system of differential equations in the variables $b_k(t) = (\mathbf{b}(t))_k$, which is readily solvable.

where $\mathcal{G}_{\max,\,\mathrm{st}} = \sup_{t\in[0,\infty)} \mathcal{G}_{\mathrm{opt},\,\mathrm{st}}(t)$. As can be seen from Fig. 11, for the case of $\alpha = 1$ and $K_\omega/K_0 = 2$, the effects of pulsatile forcing can be safely ignored beyond the upper bound of $\mathsf{Wo} \simeq 30$ on the Womersley number since in this range η is almost equal to 1, in agreement with the numerical results plotted in Fig. 10 (see Section 5).

7. Conclusions

In this paper we have re-examined the linear stability of pulsatile tube flow to axisymmetric flow perturbations. The Orr–Sommerfeld equation has been solved by means of a Galerkin projection onto a function space spanned by a finite set of the eigenfunctions of the longwave-limit Orr–Sommerfeld operator. It is shown that using few terms ($N \sim 15$–20) in the Galerkin expansion gives greater accuracy in comparison to the commonly employed Chebyshev basis. It has been found that the flow structures corresponding to the largest energy growth are toroidal vortex tubes, although non-axisymmetric disturbances may likely exists having higher energy growth. These axisymmetric vortex tubes are stretched by shear stresses of the mean flow resulting in an initial energy growth. A time of maximum energy growth is realized, and the flow perturbation subsequently decays. Maximum energy growth has been evaluated over a range of Reynolds and Womersley numbers characteristic of arterial blood flows and microfluidic applications. Asymptotic solutions provided for the longwave limit as well as the limit of large Womersley numbers agree well with the numerical results, confirming the known linear stability of the flow.

Appendix A

The operator in Eq. (11) can be factored as follows

$$\tilde{\mathcal{L}}(\tilde{\mathcal{L}} + \chi^2)\phi = 0.$$

Here, $\chi^2 = \lambda\,\mathsf{Re}$ and the general solution is given by $\phi = f_1 + f_2$ such that $\tilde{\mathcal{L}} f_1 = 0$ and $(\tilde{\mathcal{L}} + \chi^2) f_2 = 0$, i.e.

$$\phi = C_1 + C_2 r^2 + C_3 r Y_1(\chi r) + C_4 r J_1(\chi r),$$

where, respectively, $Y_1(r)$ and $J_1(r)$ are the Bessel functions of first kind [35] and C_1, C_2, C_3 and C_4 are constants to be determined by the boundary conditions. Since both the functions, $\frac{\phi}{r}$ and $\frac{1}{r}\frac{\mathrm{d}\phi}{\mathrm{d}r}$, must tend to zero as $r \to 0^+$, then $C_1 = C_3 = 0$. On the other hand, from the boundary conditions at $r = 1$, namely $\frac{\phi}{r} = \frac{1}{r}\frac{\mathrm{d}\phi}{\mathrm{d}r} = 0$, the following homogeneous linear system for the unknowns (C_2, C_4) emerges

$$\begin{cases} C_2 + J_1(\chi) C_4 = 0, \\ 2C_2 + [J_1(\chi) + \chi J_0(\chi) - J_1(\chi)] C_4 = 0. \end{cases}$$

Nontrivial solutions exist if and only if $J_2(\chi) = 0$ with $J_2(r)$ the Bessel function of first kind [35]. Consequently, there are infinitely many roots χ_n, $n = 1, 2, 3, \ldots$. The eigenvalues then readily follows as $\lambda_n = \chi_n^2/\mathsf{Re}$ and the corresponding eigenfunctions can be expressed as

$$\phi_n = c_n \left[r^2 - \frac{r J_1(\chi_n r)}{J_1(\chi_n)} \right],$$

where c_n are constants. The set $\{\phi_n\}$ is orthogonal with respect to the scalar product (13) provided one chooses $c_n = \sqrt{2}/\chi_n$.

Appendix B

The matrices defined in Eq. (17) are given by

$$\mathbf{M} = \mathbf{M}_0 + \alpha^2 \mathbf{M}_2, \quad \mathbf{K} = \mathbf{K}_0 + \alpha \mathbf{K}_1 + \alpha^2 \mathbf{K}_2 + \alpha^3 \mathbf{K}_3 + \alpha^4 \mathbf{K}_4, \quad \mathbf{H} = \alpha \mathbf{H}_1 + \alpha^3 \mathbf{H}_3. \tag{36}$$

Here, we have defined the following matrix functions

$$\begin{aligned} &\mathbf{M}_0 = \mathbf{C}(1), \qquad \mathbf{M}_2 = -\mathbf{D}(1), \\ &\mathbf{H}_1 = \mathrm{i}\big[\mathbf{D}(\tilde{\mathcal{L}} V_1) - \mathbf{C}(V_1)\big], \qquad \mathbf{H}_3 = \mathrm{i}\mathbf{D}(V_1), \\ &\mathbf{K}_0 = \mathsf{Re}^{-1}\mathbf{B}, \quad \mathbf{K}_1 = -\mathrm{i}\mathbf{C}(V_0), \quad \mathbf{K}_2 = -2\mathsf{Re}^{-1}\mathbf{C}(1), \quad \mathbf{K}_3 = \mathrm{i}\mathbf{D}(V_0), \quad \mathbf{K}_4 = \mathsf{Re}^{-1}\mathbf{D}(1), \end{aligned} \tag{37}$$

where the (n,k)-th entries of the constant matrix $\mathbf{B}$ and function matrices $\mathbf{C}(p)$, $\mathbf{D}(p)$, with $p(r) \in L_2([0,1])$, are given respectively by

$$(\mathbf{B})_{nk} = -\int_0^1 \tilde{\mathcal{L}}^2 h_k h_n \frac{\mathrm{d}r}{r}, \quad \big(\mathbf{C}(p)\big)_{nk} = -\int_0^1 p\tilde{\mathcal{L}} h_k h_n \frac{\mathrm{d}r}{r}, \quad \big(\mathbf{D}(p)\big)_{nk} = -\int_0^1 p\, h_k h_n \frac{\mathrm{d}r}{r}.$$

If Orr–Sommerfeld basis are used, $\mathbf{M}_0$, $\mathbf{K}_0$, $\mathbf{K}_2$ simplify to the following diagonal matrices

$$(\mathbf{M}_0)_{nk} = \delta_{nk}, \quad (\mathbf{K}_0)_{nk} = -\mathsf{Re}^{-1}\chi_n^2\delta_{nk}, \quad (\mathbf{K}_2)_{nk} = -2\mathsf{Re}^{-1}\delta_{nk} \tag{38}$$

since $\mathbf{C}(1) = \mathbf{I}$ and $(\mathbf{B})_{nk} = -\chi_n^2\delta_{nk}$ (δ_{nk} is the Kronecker delta).

Appendix C

Let us solve Eq. (17) by assuming the following expansion for the time-varying column vector $\mathbf{a}(t)$

$$\mathbf{a}(t) = \mathbf{a}_0(t, T_1, T_2) + \alpha\mathbf{a}_1(t, T_1, T_2) + \cdots, \tag{39}$$

where $T_1 = \alpha t$, $T_2 = \alpha^2 t$ are the advection and viscous time scales respectively. According to the multiscale method these time scales are considered independent variables. This implies that the time derivative operator is now as follows

$$\frac{\mathrm{d}}{\mathrm{d}t} = \frac{\partial}{\partial t} + \alpha\frac{\partial}{\partial T_1} + \alpha^2\frac{\partial}{\partial T_2}. \tag{40}$$

By substituting the expansion (39) for $\mathbf{a}(t)$ into Eq. (17) and using the time derivative operator (40) the following hierarchy of perturbation equations up to $\mathrm{O}(\alpha^2)$ is derived

$$\mathbf{M}_0\frac{\partial \mathbf{a}_j}{\partial t} = \mathbf{K}_0\mathbf{a}_j + \mathbf{S}_j(t), \quad j = 0, 1, 2, \tag{41}$$

where

$$\mathbf{S}_0 = \mathbf{0}, \quad \mathbf{S}_1 = \big[\mathbf{K}_1 + \mathbf{H}_1 f(t)\big]\mathbf{a}_0 - \frac{\partial \mathbf{a}_0}{\partial T_1}$$

and

$$\mathbf{S}_2 = \mathbf{K}_2\mathbf{a}_0 + \big[\mathbf{K}_1 + \mathbf{H}_1 f(t)\big]\mathbf{a}_1 - \frac{\partial \mathbf{a}_0}{\partial T_2} - \frac{\partial \mathbf{a}_1}{\partial T_1} - \mathbf{M}_2\frac{\partial \mathbf{a}_0}{\partial t}.$$

For seek of simplicity in the calculations, it is assumed that the spatial Galerkin projection has been performed using the Orr–Sommerfeld basis, implying that $\mathbf{M}_0 = \mathbf{I}$ and $\mathbf{K}_0$ is a diagonal matrix (see Appendix B). The general solution of Eq. (41) is now of the form

$$\mathbf{a}_j = \mathrm{e}^{\mathbf{K}_0 t}\mathbf{a}'_j + \mathrm{e}^{\mathbf{K}_0 t}\int_0^t \mathrm{e}^{-\mathbf{K}_0\tau}\mathbf{S}_j(\tau)\,\mathrm{d}\tau, \quad j = 0, 1, 2, \tag{42}$$

where $\mathbf{a}'_j$ determined the initial conditions (hereafter $\mathbf{b}'$ does not indicate derivatives). In particular, the $\mathrm{O}(1)$ solution is

$$\mathbf{a}_0(t, T_1, T_2) = \mathrm{e}^{\mathbf{K}_0 t}\mathbf{a}'_0(T_1, T_2), \tag{43}$$

where $\mathbf{a}'_0(T_1, T_2)$ is an unknown function of the slow time scales T_1 and T_2 to be determined. From Eqs. (42) and (43) the $\mathrm{O}(\alpha)$ solution has expression as

$$\mathbf{a}_1(t, T_1, T_2) = \mathrm{e}^{\mathbf{K}_0 t}\mathbf{a}'_1(T_1, T_2) + \mathrm{e}^{\mathbf{K}_0 t}\int_0^t \left\{\mathrm{e}^{-\mathbf{K}_0\tau}\big[\mathbf{K}_1 + \mathbf{H}_1 f(\tau)\big]\mathrm{e}^{\mathbf{K}_0\tau}\mathbf{a}'_0 - \frac{\partial \mathbf{a}'_0}{\partial T_1}\right\}\mathrm{d}\tau, \tag{44}$$

where $\mathbf{a}'_1(T_1, T_2)$ is an undetermined function. Using the Hadamard product definition, i.e. $(\mathbf{A}\circ\mathbf{B})_{ij} = (\mathbf{A})_{ij}(\mathbf{B})_{ij}$, the first term of the integrand in Eq. (44) can be written as follows

$$\mathrm{e}^{-\mathbf{K}_0\tau}\big[\mathbf{K}_1 + \mathbf{H}_1 f(\tau)\big]\mathrm{e}^{\mathbf{K}_0\tau} = \mathbf{K}_1 \circ \boldsymbol{\Gamma}_1(\tau; 0) + \mathbf{H}_1 \circ \boldsymbol{\Gamma}_1(\tau; \omega),$$

where the (i, j)-entry of the matrix of functions $\boldsymbol{\Gamma}_1$ is defined as

$$\big(\boldsymbol{\Gamma}_1(\tau;\omega)\big)_{ij} = \mathrm{e}^{(\chi_i^2/\mathrm{Re}-\chi_j^2/\mathrm{Re}+\mathrm{i}\omega)\tau}.$$

Then in Eq. (44) the secular and nonsecular terms can be readily separated as follows

$$\begin{aligned}\mathbf{a}_1(t, T_1, T_2) = \mathrm{e}^{\mathbf{K}_0 t}\mathbf{a}_1'(T_1, T_2) + \mathrm{e}^{\mathbf{K}_0 t}\int_0^t \Big\{\big[\big(\mathbf{K}_1 - \mathrm{diag}(\mathbf{K}_1)\big)\circ\boldsymbol{\Gamma}_1(\tau;0) + \mathbf{H}_1\circ\boldsymbol{\Gamma}_1(\tau;\omega)\big]\mathbf{a}_0'\Big\}\,\mathrm{d}\tau \\ + \mathrm{e}^{\mathbf{K}_0 t}\int_0^t \left[\mathrm{diag}(\mathbf{K}_1\circ\boldsymbol{\Gamma}_1(\tau;0)\mathbf{a}_0' - \frac{\partial\mathbf{a}_0'}{\partial T_1}\right]\mathrm{d}\tau. \end{aligned} \tag{45}$$

Note that the third term in Eq. (45) is of secular type $t\,\mathrm{e}^{\mathbf{K}_0 t}$; by imposing to vanish, the following equation for $\mathbf{a}_0'(T_1, T_2)$ is derived

$$\mathrm{diag}(\mathbf{K}_1)\mathbf{a}_0' - \frac{\partial\mathbf{a}_0'}{\partial T_1} = 0$$

which has the readily solution

$$\mathbf{a}_0'(T_1, T_2) = \mathrm{e}^{\mathrm{diag}(\mathbf{K}_1)T_1}\mathbf{a}_0''(T_2), \tag{46}$$

where $\mathbf{a}_0''(T_2)$ is an unknown function of the time scale T_2 to be determined. Solving the integrals in Eq. (45) gives

$$\mathbf{a}_1(t, T_1, T_2) = \mathrm{e}^{\mathbf{K}_0 t}\mathbf{a}_1'(T_1, T_2) + \mathrm{e}^{\mathbf{K}_0 t}\big[\big(\mathbf{K}_1 - \mathrm{diag}(\mathbf{K}_1)\big)\circ\Pi(t;0) + \mathbf{H}_1\circ\Pi(t;\omega)\big]\mathrm{e}^{\mathrm{diag}(\mathbf{K}_1)T_1}\mathbf{a}_0''. \tag{47}$$

Here, we have defined the matrix

$$\Pi(t;\omega) = \int_0^t \Gamma_1(\tau;\omega)\,\mathrm{d}\tau = \Pi_0(t;\omega) - \Pi_0(0;\omega)$$

and Π_0 has (i, j)-entry as

$$\big(\Pi_0(t;\omega)\big)_{ij} = \frac{\mathrm{e}^{(\chi_i^2/\mathrm{Re}-\chi_j^2/\mathrm{Re}+\mathrm{i}\omega)t}}{\chi_i^2/\mathrm{Re} - \chi_j^2/\mathrm{Re} + \mathrm{i}\omega}.$$

The governing equations for $\mathbf{a}_0''(T_2)$ and $\mathbf{a}_1'(T_1, T_2)$ are determined by imposing the vanishing of the secular terms of the $\mathrm{O}(\alpha^2)$ solution which is given by

$$\begin{aligned}\mathbf{a}_2(t, T_1, T_2) = \mathrm{e}^{\mathbf{K}_0 t}\mathbf{a}_2'(T_1, T_2) + \mathrm{e}^{\mathbf{K}_0 t}\int_0^t \Big\{&\mathbf{K}_2\circ\boldsymbol{\Gamma}_1(\tau;0)\mathrm{e}^{\mathrm{diag}(\mathbf{K}_1)T_1}\mathbf{a}_0'' + \big[\mathbf{K}_1\circ\boldsymbol{\Gamma}_1(\tau;0) + \mathbf{H}_1\circ\boldsymbol{\Gamma}_1(\tau;\omega)\big]\mathbf{a}_1' - \frac{\partial\mathbf{a}_1'}{\partial T_1} \\ &+ \big[\mathbf{K}_1\circ\boldsymbol{\Gamma}_1(\tau;0) + \mathbf{H}_1\circ\boldsymbol{\Gamma}_1(\tau;\omega)\big]\big[(\mathbf{K}_1 - \mathrm{diag}(\mathbf{K}_1)\circ\Pi(\tau;0) + \mathbf{H}_1\circ\Pi(\tau;\omega)\big]\mathrm{e}^{\mathrm{diag}(\mathbf{K}_1)T_1}\mathbf{a}_0'' \\ &- \big[(\mathbf{K}_1 - \mathrm{diag}(\mathbf{K}_1)\circ\Pi(\tau;0) + \mathbf{H}_1\circ\Pi(\tau;\omega)\big]\,\mathrm{diag}(\mathbf{K}_1)\mathrm{e}^{\mathrm{diag}(\mathbf{K}_1)T_1}\mathbf{a}_0'' \\ &- \big[(\mathbf{M}_2\mathbf{K}_0)\circ\boldsymbol{\Gamma}_1(\tau;0)\big]\mathrm{e}^{\mathrm{diag}(\mathbf{K}_1)T_1}\mathbf{a}_0'' - \mathrm{e}^{\mathrm{diag}(\mathbf{K}_1)T_1}\frac{\mathrm{d}\mathbf{a}_0''}{\mathrm{d}T_2}\Big\}\,\mathrm{d}\tau. \end{aligned} \tag{48}$$

Removing the secular terms gives the following equation for $\mathbf{a}_1'$

$$\mathrm{diag}(\mathbf{K}_1)\mathbf{a}_1' - \frac{\partial\mathbf{a}_1'}{\partial T_1} = \mathbf{S}'(T_1, T_2), \tag{49}$$

where

$$\mathbf{S}'(T_1, T_2) = -\big[\big(\mathbf{K}_1\,\mathrm{diag}(\mathbf{K}_1) - \mathrm{diag}(\mathbf{K}_1)^2\big)\circ\Pi_0(0;0) + \mathrm{diag}(\mathbf{K}_2 - \mathbf{M}_2\mathbf{K}_0)\big]\mathrm{e}^{\mathrm{diag}(\mathbf{K}_1)T_1}\mathbf{a}_0'' - \mathrm{e}^{\mathrm{diag}(\mathbf{K}_1)T_1}\frac{\mathrm{d}\mathbf{a}_0''}{\mathrm{d}T_2}.$$

Note that in Eq. (48) the secular terms depending upon the oscillatory part cancel each other exactly, implying that to the leading order the solution does not depend upon the pulsatilty of the flow. Eq. (49) admits uniform solutions if the resonance terms in the source $\mathbf{S}'(T_1, T_2)$ are removed. This gives the following equation for $\mathbf{a}_0''$

$$-\frac{\mathrm{d}\mathbf{a}_0''}{\mathrm{d}T_2} + \mathrm{diag}(\mathbf{K}_2 - \mathbf{M}_2\mathbf{K}_0)\mathbf{a}_0'' = 0$$

readily solved as

$$\mathbf{a}_0''(T_2) = \mathrm{e}^{\mathrm{diag}(\mathbf{K}_2 - \mathbf{M}_2\mathbf{K}_0)T_2}\mathbf{a}_0''', \tag{50}$$

where $\mathbf{a}_0'''$ is the vector of initial conditions. Finally from Eqs. (50), (46) and (43) the O(1) solution has the final expression

$$\mathbf{a}_0(t, T_1, T_2) = \mathrm{e}^{\mathbf{K}_0 t}\,\mathrm{e}^{\mathrm{diag}(\mathbf{K}_1)T_1}\,\mathrm{e}^{\mathrm{diag}(\mathbf{K}_2 - \mathbf{M}_2\mathbf{K}_0)T_2}\mathbf{a}_0'''.$$

The leading order solution $\mathbf{a}_0$ does not depend upon the pulsatility part and is a good approximation of the exact solution if $\alpha/\mathrm{Wo}^2 \to 0$. In this limit, the O($\alpha$) terms can be neglected.

Appendix D

Consider the function space $\mathcal{F} = \mathrm{span}(s_1, \ldots, s_n, \ldots)$ spanned by

$$s_n(r) = r^2(1 - r^2)^2 T_{2(n-1)}(r), \quad n = 1, \ldots, \tag{51}$$

where $T_{2(n-1)}(r)$ are the Chebyshev polynomials of even order defined as

$$T_{2(n-1)}(r) = \cos\big[2(n-1)\cos^{-1}(r)\big], \quad n = 0, 1, \ldots.$$

It is readily proved that the set $\{s_n\}_{n=1}^{\infty}$ satisfy the required boundary conditions and that it is orthogonal with respect to the weighted inner product

$$\langle f, g\rangle_T = \int_0^1 W(r) f g r\,\mathrm{d}r, \quad W(r) = \frac{1}{r^5(1-r^2)^4\sqrt{1-r^2}},$$

where the weight function $W(r)$ has been derived by using the normality of the set $\{T_{2n}(r)\}$ on the interval $[0, 1]$. We wish to point out that the Chebyshev basis are not orthogonal in the energy sense (i.e. with respect to the inner product 13) and as $r \to 1^-$ they do not have characteristic decay behavior as the Orr–Sommerfeld do (see Figs. 1 and 12). From Eq. (19), if one neglects the oscillatory flow component, the least stable eigenvalue of the matrix $\mathbf{M}^{-1}\mathbf{K}$ predicts the stability of the steady Poiseuille flow. Set the parameters $\alpha = 1$ and $\mathrm{Re} = 2000$. For $N = 10, 15, \ldots, 40$ the least stable eigenvalue has been evaluated by using

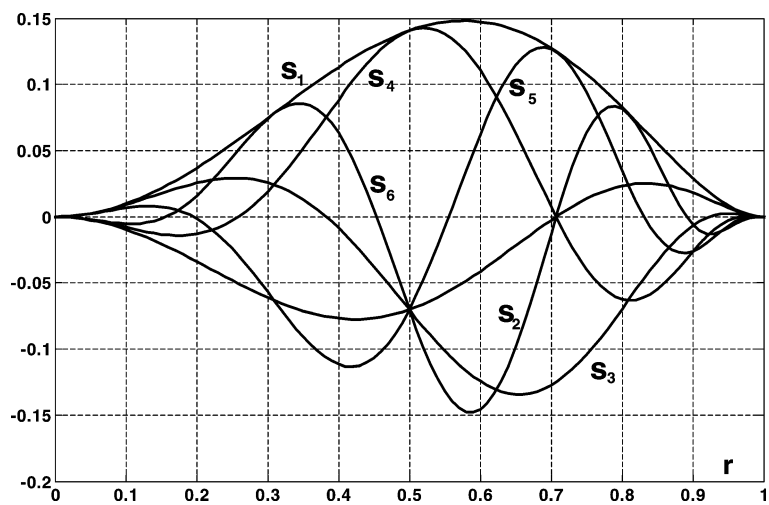

Fig. 12. The first 6 special Chebyshev basis.

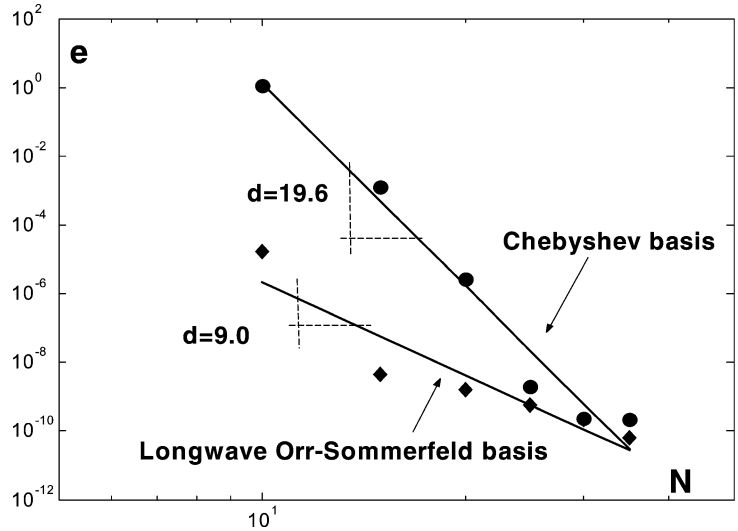

Fig. 13. Relative errors curves for the least stable eigenvalue of steady Poiseuille pipe flow for $\alpha = 1$and $\mathrm{Re} = 2000$.

both the basis $\{\phi_n\}_{n=1}^{N}$ and $\{s_n\}_{n=1}^{N}$. Taking the solution for $N = 40$ to be the 'exact' solution ($\lambda^{(40)} = -0.06375 - 0.93676\mathrm{i}$ in agreement with [27, p. 506]), the relative error

$$e = \left| \frac{\lambda^{(N)} - \lambda^{(40)}}{\lambda^{(40)}} \right| \sim N^{-d}, \quad N = 10, 15, \ldots, 35,$$

of the first least stable eigenvalue is plotted in Fig. 13. If the Chebyshev basis are used ($d = 19.6$), the error drops off faster but is always greater than the relative error if the Orr–Sommerfeld basis are used ($d = 9.0$). As an example, for $N = 15$ the error if Orr–Sommerfeld basis are used is $e \sim 10^{-8}$ whereas if the Chebyshev basis are employed, one has $e \sim 10^{-3}$.

References

[1] J.R. Womersley, Method for the calculation of velocity, rate of flow and viscous drag in arteries when the pressure gradient is known, J. Physiol. 127 (1955) 553–563.
[2] J.F. Hale, D.A. McDonald, J.R. Womersley, Velocity profiles of oscillating arterial flow with some calculations of viscous drag and the Reynolds number, J. Physiol. 128 (1955) 629–640.
[3] D.N. Ku, Blood flow in arteries, Annu. Rev. Fluid Mech. 29 (1997) 399–434.
[4] X. Geng, H. Yuan, H.N. Oguz, A. Prosperetti, Bubble-based micropump for electrically conducting liquids, J. Micromech. Microeng. 11 (2001) 270–276.
[5] K.P. Selverov, H.A. Stone, Peristaltically driven channel flows with applications toward micromixing, Phys. Fluids 13 (2001) 1837–1859.
[6] M. McGarry, D.L. Hitt, Numerical simulation of laminar mixing surfaces in converging microchannel flows, in: Computational Science & Its Applications-ICCSA 2003, in: Lecture Notes in Comput. Sci., vol. 26658, 2003, pp. 837–846.
[7] D.L. Hitt, M. McGarry, Numerical simulations of laminar mixing surfaces in pulsatile microchannel flows, J. Math. and Computers in Simul. (2003), in press.
[8] A. Davey, P.G. Drazin, The stability of Poiseuille flow in a pipe, J. Fluid Mech. 36 (1969) 209–218.
[9] L. Bergstrom, Optimal growth of small disturbances in pipe Poiseuille flow, Phys. Fluids A 5 (11) (1993) 2710–2720.
[10] L. Bergstrom, Initial algebraic growth of small angular dependent disturbances in pipe Poiseuille flow, Stud. Appl. Math. 87 (1992) 61–79.
[11] P.L. O'Sullivan, K.S. Breuer, Transient growth in circular pipe flow. I. Linear disturbances, Phys. Fluids 6 (11) (1994) 3643–3651.
[12] B.C.W. Ma, W.H. van Doorne, Z. Zhang, F.T.M. Nieuwstadt, On the spatial evolution of a wall-imposed periodic disturbance in pipe Poiseuille flow at $\mathrm{Re} = 3000$. Part 1. Subcritical disturbance, J. Fluid Mech. 398 (1999) 181–224.
[13] A.E. Gill, The least-damped disturbance to Poiseuille flow in a circular pipe, J. Fluid Mech. 61 (1973) 97–107.
[14] C.L. Dolph, D.C. Lewis, On the application of infinite systems of ordinary differential equations to perturbations of plane Poiseuille flow, Quart. Appl. Math. XVI (2) (1958) 97–110.
[15] C.E. Grosch, H. Salwen, The stability of Poiseuille flow in a pipe of circular cross-section, J. Fluid Mech. 54 (1972) 93–112.
[16] S.C. Reddy, L.N. Trefethen, Pseudospectra of the convection–diffusion operator, SIAM J. Appl. Math. 54 (6) (1994) 1634–1649.
[17] P.J. Schmid, D.S. Henningson, Optimal energy density growth in Hagen–Poiseuille flow, J. Fluid Mech. 277 (1994) 197–225.
[18] P.G. Drazin, W.H. Reid, Hydrodynamic Stability, Cambridge University Press, 1981.
[19] J.T. Tozzi, C.H. von Kerczek, The stability of oscillatory Hagen–Poiseuille flow, J. Appl. Mech. ASME 53 (1986) 187–192.

[20] P. Hall, On the instability of Stokes layers at high Reynolds numbers, J. Fluid Mech. 482 (2003) 1–15.
[21] C.E. Grosch, H. Salwen, The stability of steady and time-dependent plane Poiseuille flow, J. Fluid Mech. 34 (1968) 177–205.
[22] C.H. von Kerczek, The instability of oscillatory plane Poiseuille flow, J. Fluid Mech. 116 (1982) 91–114.
[23] C.H. von Kerczek, S.H. Davis, Linear stability theory of oscillatory Stokes layers, J. Fluid Mech. 62 (1974) 753–773.
[24] I.H. Herron, Floquet theory for the stability of boundary layer flows, J. Approx. Theory 42 (1984) 387–406.
[25] A.V. Coward, D.T. Papageorgiou, Stability of oscillatory two-phase Couette flow, J. Appl. Math. IMA 53 (1994) 75–93.
[26] S.H. Davis, The stability of time-periodic flows, An. Rev. Fluid Mech. 8 (1976) 57–74.
[27] P.J. Schmid, D.S. Hennigson, Stability and Transition in Shear Flows, Springer, 2001, pp. 556.
[28] D.S. Henningson, S.C. Reddy, On the role of linear mechanisms in transition to turbulence, Phys. Fluids 6 (3) (1994) 1396–1398.
[29] F. Waleffe, Transition in shear flows. Nonlinear normality versus non-normal linearity, Phys. Fluids 7 (12) (1995) 3060–3066.
[30] F. Waleffe, On a self-sustaining process in shear flows, Phys. Fluids 9 (4) (1997) 883–900.
[31] F. Waleffe, Hydrodynamics stability and turbulence: beyond transients to a self-sustaining process, Stud. Appl. Math. 95 (1995) 319–343.
[32] H. Wedin, R.R. Kerswell, Exact coherent structures in pipe flow: travelling wave solutions, J. Fluid Mech. 508 (2004) 333–371.
[33] H. Faisst, B. Eckhardt, Traveling waves in pipe flow, Phys. Rev. Lett. 91 (2003) 224502.
[34] B. Hof, A. Juel, T. Mullin, Scaling of the turbulence transition threshold in a pipe, Phys. Rev. Lett. 91 (2003) 244502.
[35] M. Abramowitz, I.A. Stegun, Handbook of Mathematical Functions, Dover, 1972, pp. 1046.
[36] A. Meseguer, L.N. Trefethen, Linearized pipe flow to Reynolds number 10^7, J. Comput. Phys. 186 (1) (2003) 178–197.
[37] P. Andersson, M. Berggren, D.S. Hennigson, Optimal disturbances and bypass transition in boundary layers, Phys. Fluids 11 (1) (1999) 134–149.
[38] P. Corbett, A. Bottaro, Optimal perturbations for boundary layers subject to stream-wise pressure gradient, Phys. Fluids 12 (1) (2000) 120–130.